

SCA 9210 Description of Wettability and Fluid Contacts by Using Core and Log Data.

Leif Magne Meling, Statoil
P.O Box 300
N-4001 STAVANGER Norway

Introduction

Petrophysical properties, wetting characteristics, reservoir heterogeneties and fluid migration results in an unique saturation distribution and gradient. The analysis and interpretation of this gradient gives valuable insight in the state and history of the hydrocarbon accumulation.

The initial fluid distribution versus depth is the result of the balance between the capillary and the gravitational forces. By including the informations regarding heterogeneties in the interpretation it may be possible to identify the strength of the capillary forces or the wettability of the reservoir rock. The work presented in this paper show how this can be done in a practical manner by using conventional core and log data.

Three North Sea chalk fields are studied and used as examples for description of fluid distribution, wettability, heterogeneties and hydrocarbon migration. The method presented is however general and can be used for other fields and other types of reservoirs.

Very little research has been performed to integrate core and log derived saturations. The 'J' function suggested by Lewerett (1942 and 1943)^{1, 2} has been used with success for some reservoirs. The function works well if the reservoir rock is fairly homogeneous. For heterogeneous rocks and for systems with multiple contacts, the method become difficult in use. Heseldin (1974)³ suggested an alternative approach which was further developed by Alger et. al. (1989)⁴. The Heseldin/Alger method has the disadvantage of using an empirical fit to log and core data. The estimation of fluid contacts are also somewhat impractical. If multiple fluid contacts exist, the method often fails to identify these. The method has been used by at least one oil company from the late 70 ties, some 10 years earlier then published by Alger.

Theory

At initial conditions two main forces are acting on the reservoir fluids. The gravity force separates immiscible fluids of different densities. The continuity of the fluids makes individual fluid pressure gradients and pressure differential between the phases. At equilibrium, this pressure force is balanced by the capillary force. Mathematically this can be formulated as:

$$P_c = \Delta \rho \ g \ h \quad (1)$$

Figure 1 illustrate this in a graphical manner. The system shown is water wet. The positive threshold capillary pressure or height equivalent, results in deeper free water level (FWL) than the hydrocarbon water contact (HWC). Inverse wettability will result in a higher FWL than HWC. Desbrandes and Gualdron (1988)⁵ has suggested to use this phenomena to estimate in situ wettability. The method works well if the rock has a well defined capillary entry height.

The balance of gravity and capillary forces results in a capillary pressure that must be linear with depth (except if temperature and gravity effects results in a composition gradient in the hydrocarbon phase). This important feature can be used to determine in situ wettability. If the rock types are known, capillary functions can be made to convert saturation and porosity from log to a pressure equivalent. The calculated pressures should plot on a straight line versus depth.

$$P_{cx} = \frac{(\sigma \cos \theta)_{res}}{(\sigma \cos \theta)_{lab}} P_e(\phi, k) f(S_w, S_{wi}) \quad (2)$$

The slope will be proportional to wettability, and the intercept will represent the FWL. The first term converts wetting conditions from laboratory to reservoir conditions. The second term correlates entry capillary pressure to other petrophysical parameters and the third term describes the apparent pore throat size distribution. Different types of correlations for entry capillary pressure and apparent pore throat size distribution can be used for different rock types.

Identification of rock types are the most time consuming part of the evaluation. The Brooks

and Corey (1964 and 1966)^{6, 7} equation shown below can be used for a wide range of rock types.

$$P_c = P_e S_w^{* -1/\lambda} \quad (3)$$

were:

$$S_w^* = \frac{S_w - S_{wi}}{1 - S_{wi}} \quad (4)$$

The capillary pressure can be converted to apparent pore throat radius by the following equation:

$$r = \left(\frac{\sigma \cos \phi}{P_c} \right)_{lab} \quad (5)$$

The reduced saturation can be regarded as a cumulative distribution function and the derivative as the apparent pore throat size distribution function:

$$f(r) = \frac{d S_w^*}{d r} \quad (6)$$

and

$$f(r) = \lambda r_e^{-\lambda} r^{\lambda-1} \quad (7)$$

The Brooks and Corey capillary pressure function is flexible and very useful. The distribution function are plotted for some selected values of lambda in figure 2. A lambda smaller than unity describes a porous network where a larger proportion of the pore volume are connected to smaller pore throats. A system were a larger proportion of the pore volume are connected to larger pores results in a lambda larger than unity. The special case of uniform distribution function are described by a lambda equal to unity.

Equation 2 can be rewritten as:

$$\log P_c = \log P_e - 1/\lambda \log S_w^* \quad (8)$$

Lambda and entry capillary pressure are found by plotting capillary pressure versus reduced saturation on a log-log scale. A first guess of S_{wi} is selected, a regression analysis are performed and R-squared calculated. The S_{wi} which results in a maximum value of R-squared are regarded as the correct value. The slope of the straight line represent $1/\lambda$ and the intercept P_e . By experience, a high estimate of S_{wi} by this method is often related to dual porosity at micro level as laminations, inclusions or due to non equilibrium capillary pressure data.

If the core samples are laminated some modifications can be made. If α is regarded as the volume fraction of rock 1, then the apperent pore throat distribution function can be written as:

$$f(r) = \alpha \lambda_1 r_{e1}^{(-\lambda_1)} r^{(\lambda_1-1)} + (1-\alpha)\lambda_2 r_{e2}^{-\lambda_2} r^{(\lambda_2-1)} \quad (9)$$

For shaly sands (water wett), rock type 1 can be regarded as non accessible pore volume for hydrocarbons. If the sand contain silty laminations, a more detailed description is needed. In most cases the entry radius for individual systems are distinct and easy to identify. Since equation 9 is a superposition of two distribution functions, the individual functions can be estimated by desuperposition.

The distribution function can be used to estimate average apperent pore throat and variance. The distribution function represented by equation 7 gives:

$$E(r) = \frac{r_e}{1+1/\lambda} \quad (10)$$

$$\text{Var}(r) = \frac{r_e^2}{\lambda^2+4\lambda+5+2/\lambda} \quad (11)$$

Both average apperent pore throat and variance can be used in the rock description to make correlations between different petrophysical parameters. For a given rock type, average apperent pore throat can often be correlated to porosity by a linear function. Permeability are often related to average apperent pore throat by the following equation:

$$k = \phi(1-S_{wi})E(r^2) \quad (12)$$

were:

$$E(r^2) = \frac{r_e^2}{1+2/\lambda} \quad (13)$$

Combining and rearranging equations 10 and 12 gives:

$$r_e = \sqrt{(1+2/\lambda) \frac{k}{\phi(1-S_{wi})}} \quad (14)$$

This equation is very similar to the $\sqrt{k/\phi}$ group suggested by Lewerett (1941) and supports his assumption of an "equivalent circular diameter of the voids in the sand". The $\sqrt{k/\phi}$ group is efficient to identify equivalent rock types. If lambda and irreducible wetting phase saturation are known, then the maximum percolating pore throat size can be estimated. For laminated cores, a pore throat distribution function like equation 8 should be used to calculate $E(r^2)$ and r_e .

Applications

Wettability and fluid contacts has been evaluated for three North Sea chalk fields, two condensate and one oil field. The fields are referred as field A, B and C respectively. These fields are in some areas highly fractured, but the plasticity of the chalk results in small fracture aperture and therefore moderate fracture permeability. The fields of interest include Ekofisk and Tor formations of Danian and Maatrichtian age respectively. The building block of chalk is mainly fragments of coccoliths, sceleton of planctonic algae. The size of the coccoliths of Danian age are smaller than those of Maatrichtian.

Because of chalk similarity between fields, only core data from fields A and B has been used to identify rock types. A total of 50 sets of mercury capillary pressure measurements were examined. The data are shown in figure 3. Lower porosity and thereby permeability increases the capillary entry pressure, but the shape of the capillary pressure measurements looks similar for different porosity/permeability levels. No distinct irreducible wetting phase saturation was found. Figure 4 shows the apperent pore throat size distribution function for typical Ekofisk and Tor formation samples. The data shows that the Brooks

and Corey equation describes very well the chalk studied. Regression analysis typically resulted in R-squared equal to one by three decimals. From the regression analysis lambda, entry capillary pressure and irreducible wetting phase saturation were estimated.

The results from the analysis were examined for possible relationships with other petrophysical parameters. An average lambda of 2.35 was estimated for the chalk examined, independent of other petrophysical parameters. Irreducible wetting phase saturation was found to be slightly formation dependent with a value of approximate 10 and 6 percent for Ekofisk and Tor formation respectively.

Entry capillary pressure was converted to entry pore throat by equation 5 and plotted versus porosity as shown in figure 5. A linear relationship was found for each formations as 'parallell' correlations. This is interpreted as difference in coccolithe size (grain size) between Ekofisk and Tor formations. The linear trend with porosity is belived to be a compaction and diagenetic feature. The data results in the following type correlation between entry mercury-air capillary pressure and porosity:

$$P_e = a + b\phi^{-1} \quad (15)$$

The coefficients a and b are formation dependent.

By using the rock type description for the chalk, equation 2 can be rewritten as:

$$P_{cx} = \frac{(\sigma \cos \theta)_{res}}{(\sigma \cos \theta)_{lab}} (a + b\phi^{-1}) \left[\frac{S_w - S_{wi}}{1 - S_{wi}} \right]^{-1/\lambda} \quad (16)$$

Porosity and water saturation are given from log interpretation. Saturation and calculated capillary pressure versus depth for wells from fields A and B are shown in figure 6. All wells indicate a linear capillary pressure versus depth. The intercept at zero capillary pressure estimates the free water level and the slope the wettability. Some wells penetrates major faults and fractures. A stepwise change in calculated capillary pressure versus depth are often observed across these faults and fractures.

The interpretation of wettability are shown in figures 7 and 8. The condensate fields are evaluated to be strongly water wett with a $\sigma \cos\theta$ of approximate 40 mN/m. For the oil fields however, the data indicates a very weak capillary force. A $\sigma \cos\theta$ in order of 0.02

mN/m indicates intermediate wetting. This is comparable with the results published by Cuiec (1987)⁸ for the same fields.

The FWL was examined in detail for field A. Figure 6 shows the saturation versus depth for four wells and the calculated capillary pressure versus depth. Each individual well shows individual FWL. The difference between wells are significant, up to 200 m. The deepest contacts are found in flank wells and the shallow contacts are found at the crest of the structure. This phenomena is believed to be related the fracture network and to migration of hydrocarbons through these into the structure.

Fluid distribution

Up to now a simple hydrocarbon distribution model suggested by D`Heur (1984)⁹ has been used for the North Sea chalk reservoirs. The model suggests that saturations are controlled by the porosity and permeability reduction downflank. Variations in fluid saturations between different well locations at comparable depth and porosity-permeability values, has been explained by changes in rock types. The analysis of fluid distribution for field A suggest other mechanisms responsible for the difference in FWL's.

Fractures and fracture direction has been studied in detail for field A and published by Lehne and Aadnøy (1990)¹⁰. FWL's estimated from logs (a total of 8 wells) shows that the 'FWL gradient' is perpendicular to the direction of fractures and are showing that fractures are the main heterogeneity regarding saturations. The data also shows that only a small proportion of the fractures observed in the wells are percolating and influence the saturation profile. A similar conclusion regarding the fracture network has been presented by Hamon (1991)¹¹. For a major oil chalk field, he used well test analysis and reservoir simulation history matching and came to the same conclusion.

The fluid distribution model is shown in figure 9. Major fractures, probable related to fault systems, makes a percolating network. Hydrocarbons migrate into this network and displace water, first from the fractures and secondly from the matrix. The pressure differential between the phases are the driving force and the strength is dependent on the height of the matrix block, the density difference and the hydrocarbon water contact in the fracture system. If the fluid contact in the fracture system drops below the bottom of the matrix block, the wetting phase become isolated and a maximum driving force is obtained. The

maximum pressure differential is located at the top of the matrix blocks. If this pressure differential is exceeding the entry pressure for the matrix, water is displaced by hydrocarbons. By this mechanism, the FWL is related to bottom of the matrix block and thereby to the degree of fracturing. Down structure wells may have significant deeper contact than chestal wells if the fluid contact in the fracture network is deep. If the degree of fracturing vary across the field, the FWL estimated by logs would be shallower in highly fractured areas. This is due to the reduction in matrix block height in highly fractured areas. Several North sea chalk fields seems to have this feature⁹. Even more complicated systems may occur. Since only a small proportion of the fractures seems to make a percolating network, some areas may have a local fracture systems with separate fluid contact in the fractures. Such a system can be directly related to the migration of hydrocarbons into the structure.

Fluid migration

The fluid distribution for field A opens a new insight to fluid migration into the field. Figure10 describe in a schematic way the structural geology for some fields in the Ekofisk Area. The source rocks are Upper Jurassic shales. The Shale is very thick with interbedded sand intervals. The pressure in the Jurassic and underlying Triassic sands are close to lithostatic, equivalent to a mud weight of 2 g/cm³. The underlying Zechstein salt makes salt pillows or diapirs within grabens and salt walls associated with faulting. The overlying chalk group have a lower pressure, typically equivalent to a mud weight of 1.6 g/cm³. The the lack of pressure communication is due to marls and shales in the Lower Createous and the shales in the Upper Jurassic and indicates an efficient barrier between the source rocks and the reservoirs. The conditions above strongly suggest a fault valve mechanism responsible for migration.

The fault valve behaviour is described by Sibson (1990)¹². A fault valve can be described as follows: (1) build-up of pressure below an impermeable barrier, (2) break down and reactivation of older faults, (3) rupture of fluid to the overburden, (4) the pressure across the barrier equalises, (5) the fault closes and a new cycle begins. The pressure increase can be due to thermal heating, tectonic compaction, dehydration or generation of hydrocarbons. For the Ekofisk Area the most probable reason is generation of hydrocarbons since the large pressure differential exist between the reservoir and the source rock. The reactivated faults are probably those associated to the salt pillows and diapirs.

The process discussed above lead to migration through faults and associated fractures into the structures. Each individual fault block will behave as a separate system. The water phase in the fault blocks will be totally isolated by the hydrocarbon filled faults and fractures. The degree of filling will be dependent on total amount of hydrocarbons migrated into the structure, fracture intensity, degree of fracture continuity and hydrocarbon volumes transported through individual fault and fracture systems.

Conclusions

The conclusions can be summarize as:

1. In situ wettability can be predicted by using a quantitative rock type description method of reservoir cores in the evaluation of saturation gradients from well logs.
2. For North Sea chalks, the Brooks and Corey equation describes very well most rock types.
3. Several of the fractured chalk fields have multiple hydrocarbon water contacts on macro scale probably due to fracture systems.
4. The fault and fracture system makes the wetting phase non continuous.
5. In situ wettability $\sigma \cos\theta$ for the gas condensate systems are estimated to approximate 40 mN/m (dyn). This correspond to a strong water wet system.
6. The oil fields indicate a very weak water wet system with a $\sigma \cos\theta$ in the order of 0.02 mN/m (dyn).
7. Fault valve behaviour is probably an important process in migration of hydrocarbons into the Ekofisk Area structures.

Acknowledgments

Without the support from my family, my wife Tove and our three children, this work would not been put on paper.

Nomenclature

a	= Correlation coefficient.
b	= Correlation coefficient.
dS_w^*	= Derivative of reduced wetting saturation.
dr	= Derivative of apparent pore throat size.
E(r)	= Average apparent pore throat ($\mu\text{-m}$).
E(r ²)	= Average apparent pore throat squared ($\mu\text{-m}^2$).
f(r)	= Apparent pore throat distribution function.
g	= Gravitational constant (N/s^2).
h	= Thickness (m).
k	= Permeability ($\mu\text{-m}^2$).
lab	= Laboratory conditions.
P_c	= Capillary pressure (Bar)
P_{cx}	= Capillary pressure function (Bar).
P_e	= Entry capillary pressure (Bar).
r	= Apparent pore throat radius ($\mu\text{-m}$)
r_e	= Maximum apparent pore throat radius ($\mu\text{-m}$).
res	= Reservoir conditions.
S_w	= Water saturation (-).
S_{wi}	= Initial water saturation (-).
S_w^*	= Reduced water saturation (-)
Var(r)	= Variance of apparent pore throat size ($\mu\text{-m}$).
α	= Volume fraction (-).
$\Delta \rho$	= Density difference (g/cc).
ϕ	= Porosity (fraction).
λ	= Apparent pore throat size distribution coefficient (-).
σ	= Surface tension (mN/m).

References

1. Lewerett, M.C., (1942), Capillary Behaviour in Porous Solids *Trans*, AIME, 142,151-69.
2. Lewerett, M.C., Lewis, W.B. and True, M.E., (1942), Dimensional Studies of Oil-Field Behaviour, *Trans.* , AIME,146, 175-93.
3. Heseldin, G.M., (1974), A Method of Averaging Capillary Pressure Curves, *Proc.*, 1974 SPWLA Annual Logging Symposium (June 2-5), paper E.
4. Alger, R.P., Luffel, D.L., Truman, R.B.,1989, New Unified Method of Integrating Core Capillary Pressure Data With Well Logs, *SPE Formation Evaluation* (June 1989), 145-152.
5. Desbrandes, R., Gualdrón, J., 1988, In situ Rock Wettability Determination with Wireline Formation Tester Data, *The log Analyst* (July-August, 1988), 244-252.
6. Brooks, R.H. and Cory, A.T., 1964, Hydraulic Properties of Porous Media, *Hydraulic Paper Number 3*, Colorado State University.
7. Brooks, R.H. and Corey, A.T., 1966, Properties of Porous Media Affecting Fluid Flow, *Journal of the Irrigation and Drainage Division*, Proc. of ASCE , vol. 92, No. IR2, pages 61-88.
8. Cuieq,L., Wettability and oil reservoirs,1987, *North Sea Oil and Gas Reservoirs*, Graham and Trotman , pages 193-207.
9. D`Heur, M, 1984, Porosity and hydrocarbon distribution in the North Sea chalk reservoirs, *Marine and Petroleum Geology* (August 1984), Volume 1, pages 211-238.
10. Lehne,K. A., Aadnøy, S. B., 1990, Quantitative Analysis of Stress Regimes and Fractures from logs and Drilling Records of A North Sea Chalk Field,"*SPWLA 13th European Symposium*, Budapest Hungary (October 1990), paper P.
11. Hamon, G., 1991, The Effect of Fracture Permeability Distribution on Waterflood Efficiency in Naturally Fractured Reservoirs, *Sixth European Symposium on Improved Oil Recovery* (21-23 May 1991), Proceedings Volume 1 ,pages 417-425
12. Sibson, R. H., 1990, Conditions for fault valve behaviour, *Deformation Mechanisms Rheology and Tectonics*, The Geological Society (1990), pages 15-28.

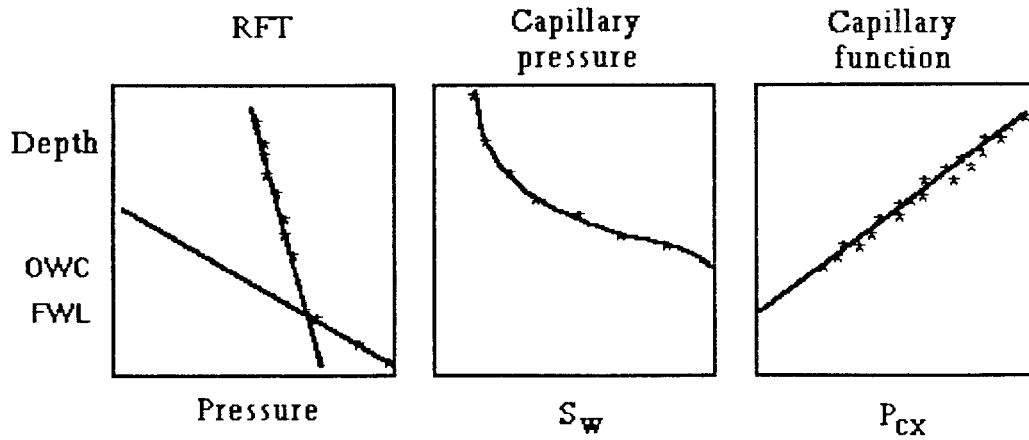


Figure 1. Capillary pressure versus depth.

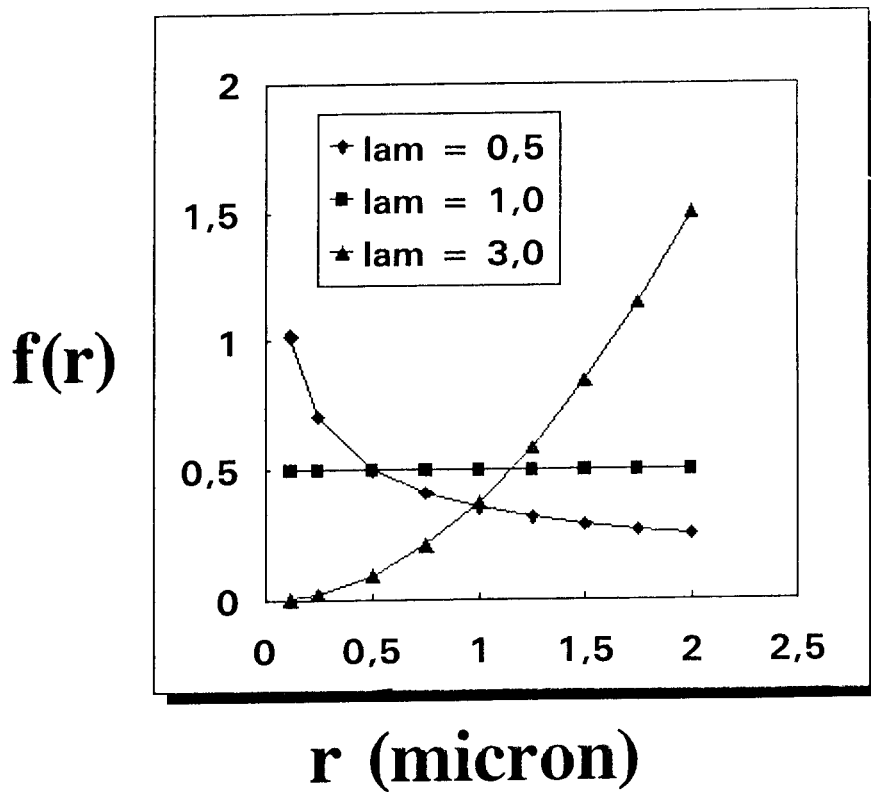


Figure 2. The Brooks and Corey capillary pressure function.

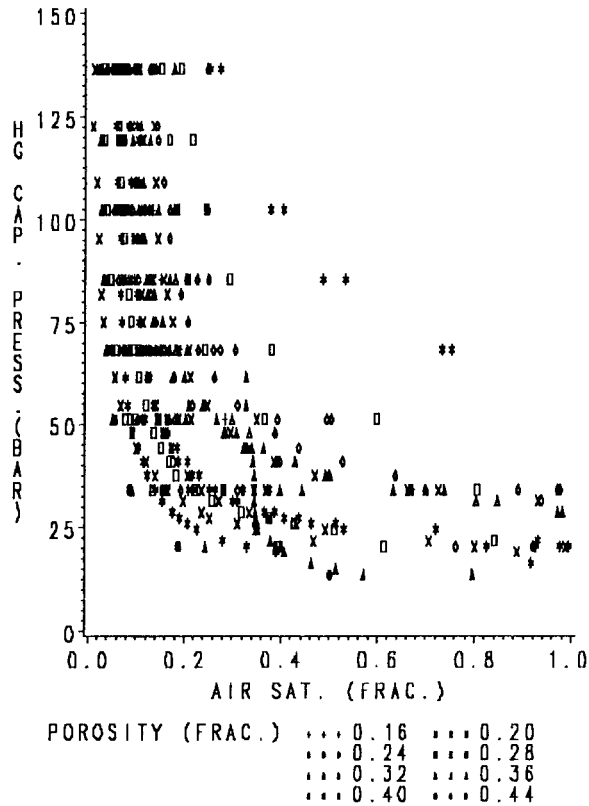


Figure 3. Mercury capillary pressure measurements for field A and B.

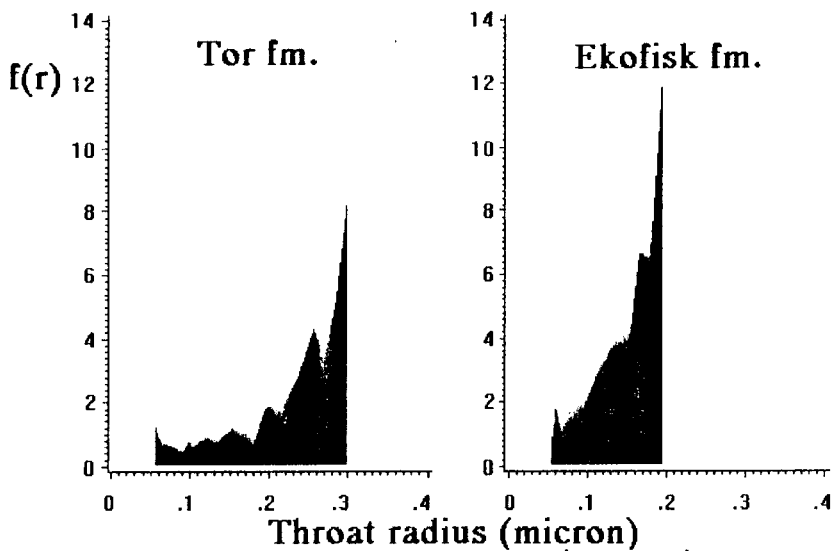


Figure 4. Apparent pore throat size distribution, Ekofisk and Tor formations.

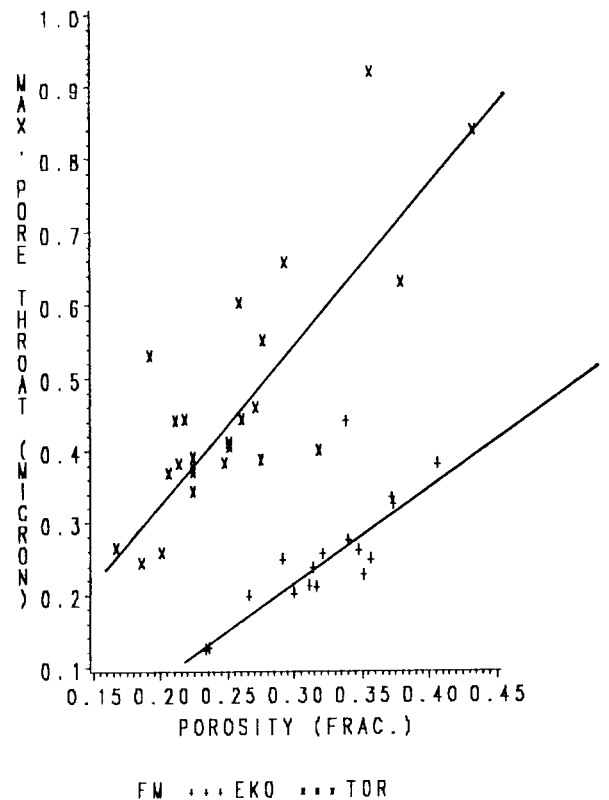


Figure 5. Maximum percolating pore throat radius.

Water Saturations and Pcx Field A and B

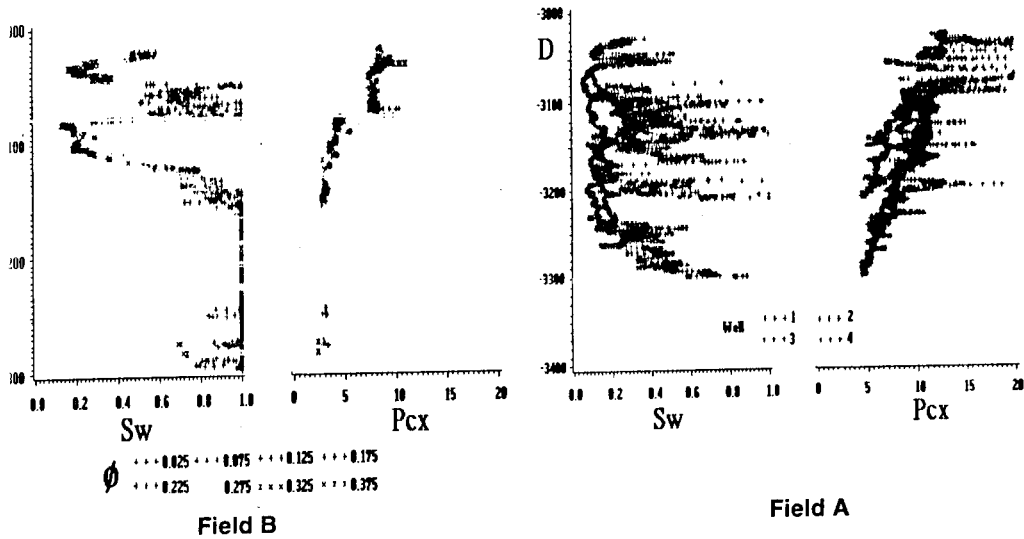
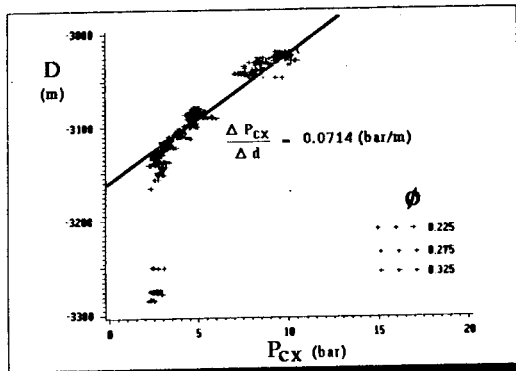


Figure 6. Saturation and calculated capillary pressure versus depth for fields A and B.

Determination of Wettability Field B



Fluid data:

- ▲ gas-condensate
- ▲ $\Delta\rho = 1.05 - 0.42 = 0.63 \text{ g/ cm}^3$
- ▲ $\Delta P/ \Delta d = 0.062 \text{ (bar/ m)}$

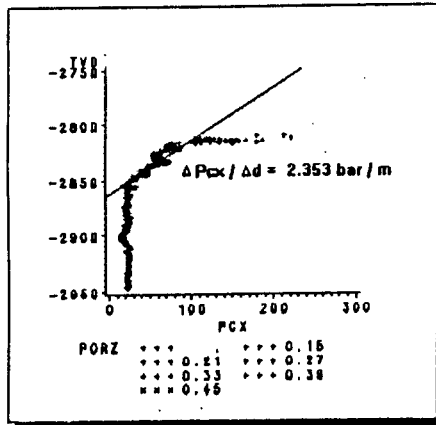
Pcx analysis:

- ▲ assumed $\sigma \cos \theta = 50 \text{ mN/m}$
- ▲ $\Delta P_{cx}/ \Delta d = 0.0714 \text{ (bar/ m)}$

Real $\sigma \cos \theta$: $50 * 0.062/ 0.0714 = 43 \text{ mN/m}$

Figure 7. Estimation of wettability field B.

Determination of Wettability Field C



Fluid data:

- ▲ light oil
- ▲ $\Delta\rho = 1.05 - 0.60 = 0.45 \text{ g/cm}^3$
- ▲ $\Delta P / \Delta d = 0.044 \text{ (bar/m)}$

Pcx analysis:

- ▲ assumed $\sigma \cos \theta = 1 \text{ mN/m}$
- ▲ $\Delta P_{cx} / \Delta d = 2.353 \text{ (bar/m)}$

Real $\sigma \cos \theta$: $0.044 / 2.353 = 0.019 \text{ mN/m}$

Figure 8. Estimation of wettability field C.

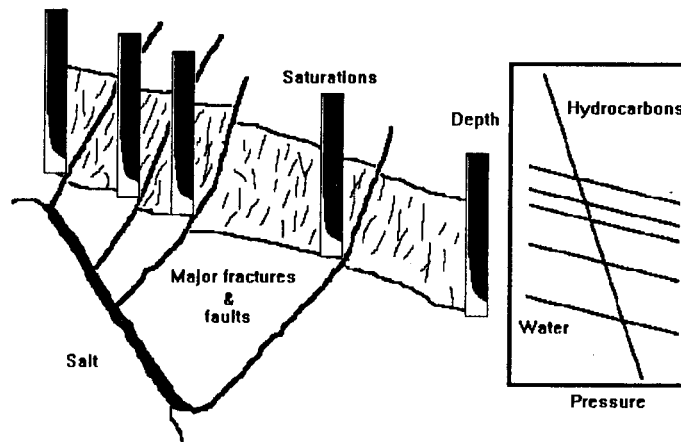


Figure 9. Fluid distribution model.

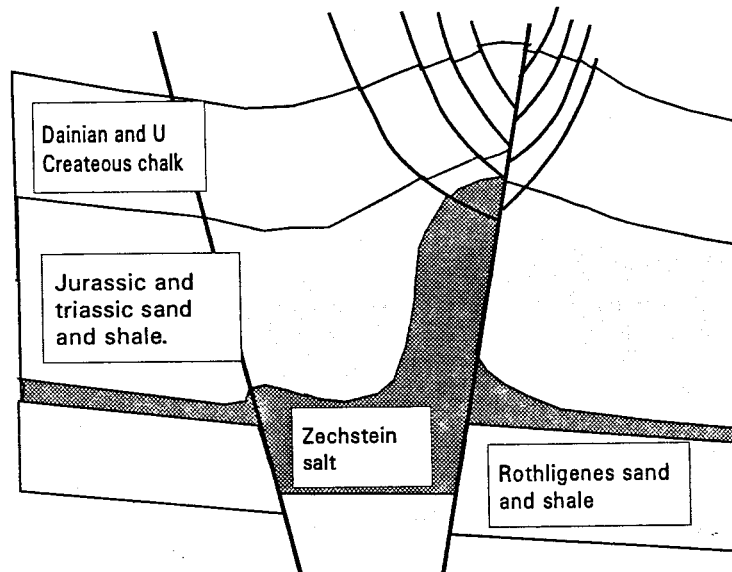


Figure 10. Structural geology for some structures in the Ekofisk Area.

